Self-Assembly of Synthetic Cellulose during in-Vitro Enzymatic Polymerization Process As Studied by a Combined Small-Angle Scattering Method

Hirokazu Tanaka,[†,‡] Satoshi Koizumi,*[,†] Takeji Hashimoto,*[,†,‡] Kazuhiro Kurosaki,[§] and Shiro Kobayashi[⊥,§]

Advanced Science Research Center (ASRC), Japan Atomic Energy Agency (JAEA), Tokai, Ibaraki 319-1195, Japan; Department of Polymer Chemistry, Graduate School of Engineering, Kyoto University, Katsura, Kyoto 615-8510, Japan; and Department of Materials Chemistry, Graduate School of Engineering, Kyoto University, Katsura, Kyoto 615-8510, Japan

Received March 22, 2007; Revised Manuscript Received June 6, 2007

ABSTRACT: We have investigated the self-assembling process of cellulose artificially synthesized via enzymatic polymerization as one of general problems of chemical reactions at specific sites and reaction-induced self-assembling process of reaction products in the context of nonequilibrium phenomenon and pattern formation. The chemical reaction and the self-assembling process were explored at real time and in-situ by a combined small-angle neutron scattering (SANS), small-angle X-ray scattering (SAXS), ultra-SANS, and ultra-SAXS method, together with wide-angle X-ray diffraction and field-emission scanning electron microscopy. The results revealed the following pieces of new evidence: (i) Even in the aqueous reaction medium free from monomers, enzymes (cellulase) as a catalyst aggregate themselves into associations with characteristic lengths larger than 200 nm. (ii) Cellulose molecules created at each active site of enzymes associate themselves around the enzyme associations into cellulose aggregates having surface fractal dimensions D_s, increasing from 2 to 2.3 with reaction time. (iii) The fractal structure formed at the end of the reaction extends over a surprisingly wide length scale ranging from ∼30 nm to ∼30 μm (3 orders of magnitude). This unique self-assembly of the reaction products is proposed to be caused by the following factors: (a) an extremely large number of polymers are repeatedly created at an active center of the catalyst in the enzyme association; (b) the polymers formed keep springing out from the narrow space in the catalyst, where the active center locates, toward the reaction medium where (c) the polymers formed associate themselves into aggregates because they are insoluble in the medium.

I. Introduction

Aim of This Study. As far as we know, there are almost no reports that challenge to elucidate a self-assembling process of cellulose molecules synthesized in-vitro at specific reaction sites of an enzyme by means of a combined small-angle scattering (SAS) method. We consider the self-assembled structures and the self-assembling process, which are denoted hereafter as self-assembly, as one of general problems in macromolecules, concerning reactions at specific sites (an active site of an enzyme in this study) and self-assembling of reaction products (polymers) into supermolecular structures (supermolecular structure of cellulose fibrils in this study). This paper is aimed to give a full account of the works presented previously as a short communication.[1]

The study aims also to clarify nonequilibrium pathways for self-organizations of macromolecular assemblies in one of the so-called open nonequilibrium systems which are exposed to external energy flow. The studies of open nonequilibrium systems are believed to be important for understanding not only pattern formation in nature but also dynamics and activities of various structural elements in living biological systems. In the particular system to be considered in this work, an energy for a chemical reaction is given to the system of interest via a mixing of an enzyme solution and a substrate monomer solution: as a consequence of the energy given to the system, the system keeps creating cellulose molecules from the specific active sites of the enzyme, and the molecules keep being self-assembled in the system. Hopefully, we like to elucidate some physical factors which control the chemical reaction at specific sites and to suggest a hint which may be useful in order to attain an increased degree of polymerization (DP) and to control crystal structure of the artificially synthesized cellulose.

The combined SAS method, involving small-angle neutron scattering (SANS), ultra-SANS (USANS), small-angle X-ray scattering (SAXS), and ultra-SAXS (USAXS), together with wide-angle X-ray scattering (WAXS) method enabled us to systematically unveil the self-assembly of the reaction products over an extremely wide length scale, ranging from ∼0.1 nm to ∼30 μm. Furthermore, the method was combined by a real-space method of field-emission scanning electron microscopy (FE-SEM). We report the work that succeeded in elucidating the reaction-induced self-assembling process and structure of artificially synthesized cellulose molecules.

General Features of Cellulose Synthesis. In-vitro synthesis of cellulose has long been one of the most challenging research subjects. Almost all trials, however, failed to overcome difficulties in attaining a precise control of the regio- and stereoselective reaction to form a β-1,4-glycocidic linkage.[2−6] As for the biosynthetic pathway, we can find some reports that lead to successful formation of the synthetic cellulose by using *Acetobacter xylinum* or *Phaseolus aureus* and nucleoside diphosphate sugar (ADP-, CDP-, or GDP-glucose) as substrate monomers.[7,8] As for the nonbiosynthetic pathway, the first

* To whom correspondence should be addressed.
† Japan Atomic Energy Agency.
‡ Department of Polymer Chemistry, Kyoto University.
§ Department of Materials Chemistry, Kyoto University.
⊥ Present address: R & D Center for Bio-based Materials, Kyoto Institute of Technology, Kyoto 606-8585, Japan.

10.1021/ma070699u CCC: $37.00
Published on Web 07/31/2007

Scheme 1. Reaction Scheme for Enzymatic Polymerization To Synthesize Cellulose

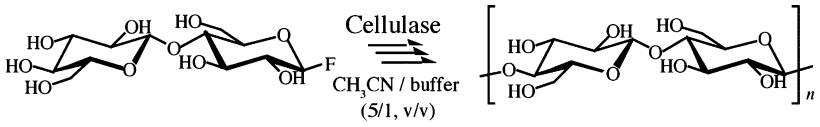

successful reaction to obtain the synthetic cellulose via "enzymatic polymerization" was reported in 1991.[9] However, the number-average degree of polymerization, DP, of the obtained cellulose molecules was about 11 in terms of monomeric unit of cellobiose (or 22 in terms of glucose units), though this value was the largest one obtained so far via the in-vitro synthesis.[10]

Enzymatic Polymerization to Cellulose. The "enzymatic polymerization" to cellulose was defined as in-vitro polymerization catalyzed by isolated enzymes via a nonbiosynthetic pathway.[11,12] The polymerization used cellobiose having a fluoride group at its anomeric position as an activated substrate monomer and a mixture of organic and aqueous solvent as a reaction medium, as schematically shown in Scheme 1. By using the mixed solvents and optimizing pH of the solution, the equilibrium reaction was shifted toward the polymerization reaction rather than the hydrolysis reaction. One of the most important points of this method is that one can obtain regio- and stereocontrolled cellulose via only a one-step chemical reaction involving the elimination of HF.

The simple synthetic method makes in-situ observation of the self-assembly of reaction products in the polymerization process feasible. It was also found that cellulose thus synthesized self-assembled to form spherulitic crystalline superstructures in the course of the polymerization process.[13] In addition, it is elucidated that the crystal structure in the synthetic cellulose changed, depending on the purity of cellulase.[14] With an unpurified enzyme a thermodynamically stable crystal form, cellulose II, was formed, while with a partially purified enzyme a thermodynamically metastable crystal form, cellulose I, as well as the cellulose II were formed. For a better understanding of these intriguing experimental results, it would be quite important to investigate the self-assembling processes of cellulose during the enzymatic polymerization process.

Importance of in-Situ and Real-Time SANS Measurements. Since neutron has excellent transmittance and very low quantum energy ($\sim 10^{-4}$ keV) compared to X-rays ($\sim$10 keV), we can apply the SANS to reaction systems without causing radiation-induced side reactions, to living biological systems such as *Acetobacter xylinum*[7] producing cellulose without severe radiation damages, to systems with high turbidity for light, and to systems having high absorption coefficients for light and X-rays. The SANS can usually probe structures and sizes of molecules or molecular assembly in the length scale ranging from 1 to 100 nm. The method can be reinforced by combining other SAS methods described earlier, as will be highlighted in this work.

II. Experimental Section

II.1. Enzymatic Polymerization. In this work the in-vitro, enzymatic synthesis of cellulose was performed according to the method previously described.[9] The details of the method are as follows: A substrate monomer of β-cellobiosyl fluoride first synthesized and purified (10.3 mg, 2.9×10^{-5} mol; purity 95%) was solubilized in 170 μL of acetate buffer in D_2O (CH_3COOH/CH_3COONa/D_2O) (pD = 5.0, 0.05 M). To this solution was added acetonitrile (1000 μL). Deuterated molecules were used to enhance the scattering contrast for the self-assembled cellulose molecules and enzymes against the reaction medium as well as to reduce the incoherent scattering intensity level. The polymerization was started by mixing, as shown in Figure 1, the above solution, designated as solution A, with 30 μL of acetate buffer in D_2O (pD = 5.0, 0.05 M) containing unpurified cellulase (originated from *Trichoderma viride*; 0.52 mg, 5 wt % per unit weight of the substrate monomer), designated as solution B. Among various cellulase components, endglucanase (EG1 and EG2) was an active component. The reaction system had a total volume of 1200 μL (acetonitrile/buffer = 5/1 v/v) and a monomer concentration of 0.025 M.

The polymerization temperature was set at 30 °C. The reaction solution was translucent up to 2 h after mixing, but it gradually became opaque and turbid. As the reaction further proceeded, a white precipitate of the reaction product (polysaccharide) appeared in the solution, indicating that the polymerization successfully proceeded. At 24 h after the onset of the polymerization, the reaction solution was heated in boiled water at 80 °C for 10 min to terminate the polymerization via inactivation of enzyme activity. The reaction-terminated solution was then used for further characterization of the following items at the end of the polymerization reaction: (i) molecular weight of the synthesized cellulose molecules via SEC (size exclusion chromatography), (ii) monomer conversion via HPLC (high performance liquid chromatography), and (iii) the self-assembled structures of cellulose molecules via USANS, USAXS, SANS, SAXS, WAXS, and FE-SEM. We confirmed the inactivation did not cause any changes at all in the self-assembled structures of the reaction products by using the combined USANS and SANS method.[15]

II.2. Characterization of the Polymerization Process and the Reaction Product. II.2.1. HPLC. In order to investigate the time dependence of monomer conversion, $C_M(t)$, during the polymerization process, HPLC measurements were conducted (HPLC; LC8020 system, Tosoh, Tokyo, Japan). Monomer conversion, $C_M(t)$, is defined as

$$C_M(t) = \frac{w(t=0) - w(t)}{w(t=0)} \times 100 \qquad (1)$$

where $w(t=0)$ and $w(t)$ indicate weight of monomers existing in the reaction solution at $t = 0$ and t, respectively. The reaction at a given t was terminated as described in section II.1. Then, solvent was evaporated under a reduced pressure in order to separate acetonitrile from the monomers, as HPLC peaks from acetonitrile and monomers overlap each other. It is noted here that the obtained products contain both synthesized cellulose molecules and unreacted monomers, as monomers do not evaporate. In order to separate the two components, the obtained products were resuspended in 300 μL of distilled water for HPLC. Thus, unreacted monomers were dissolved in the eluents, and synthesized cellulose molecules remained insoluble in the eluents. Then, in order to remove cellulose molecules, the samples were filtered, and only unreacted monomers were injected into the HPLC port to evaluate $w(t)$.

II.2.2. SEC. The molecular weight of the product was determined by SEC measurement (GPC8020 with Tosoh α-3000 column diameter 7.8 × 300 mm, Tosoh, Tokyo, Japan) eluting with 600 mM LiCl in *N*-methyl-2-pyrrolidone/*N*,*N*-dimethylacetamide (LiCl−NMP/DMAc) (2/1, v/v) mixed solution (flow rate, 0.6 mL/min, Tosoh, Tokyo, Japan; 65 °C). For calibration of the relationship between molecular weight and elution time, pullulan standards and three cellooligosaccharides having sugar units of 2, 4, and 6 were also measured.

II.2.3. Time-Resolved SANS Measurement. As schematically shown in Figure 1, immediately after starting enzymatic polymerization by mixing the two solutions A and B in a quartz cell with thickness of 2 mm, the cell was quickly mounted on a sample stage for a time-resolved SANS measurement. The time was set to be

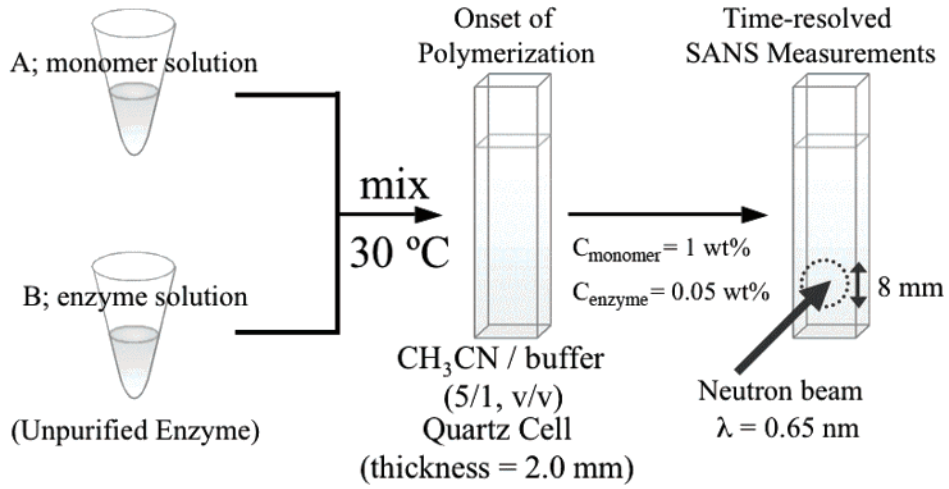

Figure 1. Experimental procedure for time-resolved SANS measurement.

zero at the time when the two solutions were mixed together. During the measurement, the cell was precisely kept at 30 °C with a precision of ±0.5 °C. The time-resolved SANS measurement was conducted with SANS-J spectrometer installed at JRR-3 (Japan Research Reactor-3) in JAEA (Japan Atomic Energy Agency), Tokai, Japan. The wavelength, λ, of the incident neutron beam was 0.65 nm and had a distribution of λ ($\Delta\lambda$) as characterized by $\Delta\lambda/\lambda = 0.12$. The scattered neutrons were detected by a two-dimensional ^{3}He position-sensitive detector of 0.58 m diameter, and circularly averaged scattered intensity was obtained as a function of q, where q is a magnitude of the scattering vector, defined by

$$q = (4\pi/\lambda)\sin(\theta/2) \tag{2}$$

with θ being the scattering angle. SANS-J covered a q-range of $3 \times 10^{-2} < q < 3$ nm^{-1}, corresponding to length scale $r \equiv 2\pi/q$ of 2 nm $< r <$ 200 nm. The obtained scattered intensity was corrected for background scattering, electronic noise of detector, detector sensitivity, and transmission and then converted to an absolute intensity scale (cm^{-1}) using a porous aluminum plate as a secondary standard.

II.2.4. USANS Measurement. For an analysis of the self-assembly at the length scale r larger than 200 nm, a Bonse-Hart type[16] USANS apparatus was used (PNO spectrometer installed at JRR-3 in JAEA, Tokai, Japan). The PNO spectrometer covered q-range of ultrasmall scattering angle ($2 \times 10^{-4} < q < 1 \times 10^{-2}$ nm^{-1}, corresponding to 600 nm $< r <$ 30 μm) using monochromatized neutron beam ($\lambda = 0.2$ nm), as detailed elsewhere.[17] The scattering profiles obtained by PNO were corrected for background scattering, transmission, slit height smearing according to the infinite beam height assumption, and slit width smearing. Finally, the absolute scattered intensity of the USANS profile was calibrated by shifting the USANS profile plotted in $\log(d\Sigma/d\Omega(q))$ vs $\log(q)$ along intensity scale to adjust the absolute intensity level of the SANS profile also plotted in $\log(d\Sigma/d\Omega(q))$ vs $\log(q)$ where $d\Sigma/d\Omega(q)$ designates differential scattering cross section. The shifting USANS profile relative to the SANS profile is straightforward because both obeyed the same power law as shown in Figure 9.

II.2.5. USAXS and SAXS Measurements. To cover q-range, which cannot be accurately measured by SANS and USANS as will be detailed in section III, we performed USAXS and SAXS measurements. USAXS measurements were performed with a Bonse-Hart type[16] USAXS apparatus, the details of which are described elsewhere.[18] The q-range covered by USAXS was $2 \times 10^{-3} < q < 9 \times 10^{-2}$ nm^{-1}, corresponding to 70 nm $< r < 3$ μm. SAXS measurements were performed with the SAXS apparatus which consists of an 18 kW rotating-anode X-ray generator (Bruker AXS K. K., Yokohama, Japan), a graphite crystal for incident-beam monochromatization ($\lambda = 0.154$ nm), and a one-dimensional position-sensitive proportional counter (PSPC).[19] The SAXS profile was obtained with a camera length of 1200 mm in order to cover the q-range of $0.2 < q < 2$ nm^{-1}, corresponding to 3 nm $< r <$ 30 nm.

The USAXS and SAXS profiles were corrected for background scattering and slit height and width smearing. Finally, the scattered intensity profiles for both USAXS and SAXS in the double-logarithmic scale were shifted toward the absolute intensity of the USANS and SANS profiles in the double-logarithmic scale with a sufficient overlapping q-range for each, as clearly shown in Figure 10.

II.2.6. WAXS Measurements. To investigate crystal structure of the synthesized cellulose, WAXS measurements were conducted. The details of the WAXS apparatus are described elsewhere.[19,20] The diffraction angle, 2θ, covered by WAXS was between 10° and 30° arc. The WAXS data were corrected for background (empty cell) and transmission.

II.2.7. FE-SEM Observations. For a real-space analysis of both associations of enzyme themselves and those of the synthesized cellulose, FE-SEM observations were performed. In order to observe structures of enzyme associations, we prepared exactly the same enzyme solutions as that used for enzymatic polymerization system described in section II-1, except for the absence of monomers. The enzyme solution was then placed on a flat silicon substrate, and solvent was evaporated gradually at room temperature under atmospheric pressure. The solvent-insoluble white precipitates in the reaction medium were also placed on a flat silicon substrate. Prior to FE-SEM observations, the sample surface was sputter-coated by platinum atoms for 2 min under sufficiently low pressure. FE-SEM observations were performed with JEOL JSM-6335F at accelerated voltage of 10 kV.

III. Results

III.1. SEC Measurements. The number-averaged molecular weight, M_n, of the product was determined to be 1840 and therefore the number-average DP = 5.7 in terms of cellobiose monomeric unit (corresponding to 11.4 glucose units).

III.2. HPLC Analysis. $C_M(t)$ as determined by HPLC analysis is shown by filled squares in Figures 4 and 8. It is found that $C_M(t)$ increased with increasing reaction time and reached a finite value of 75% at $t = 1020$ min. Thus, again, it is confirmed that enzymatic polymerization in this study proceeded successfully.

III.3. WAXS Measurement. The results for WAXS measurements are shown in Figure 10. Three obvious peaks appeared at $2\theta = 11.6°$, 19.8°, and 22.0° arc, which are well consistent with the diffraction pattern observed for the crystal structure of cellulose II, the thermodynamically stable form.[21]

III.4. SANS Measurements. III.4.1. SANS from Enzyme Solution. The structure of enzyme solution itself, containing

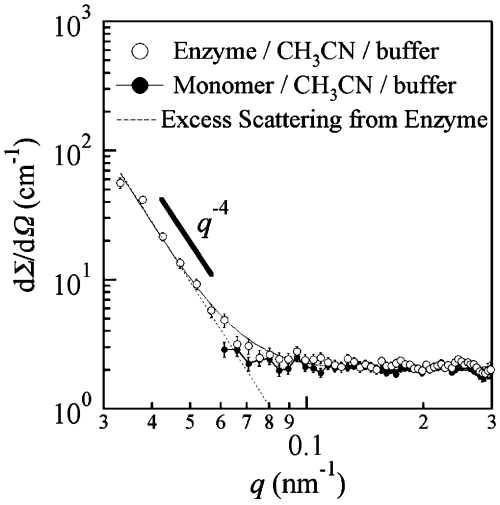

Figure 2. SANS profiles for enzyme solution (enzyme/CH_3CN/buffer) and reaction medium (monomer/CH_3CN/buffer).

CH_3CN by the same amount as the reaction solution, before enzymatic polymerization was characterized in-situ by SANS. The result is shown by open circles in Figure 2 where the absolute scattered intensity (differential scattering cross section) $d\Sigma/d\Omega(q)$ was double-logarithmically plotted as a function of q. At higher q-region of $q > 0.1$ nm^{-1}, almost q-independent scattering was observed, which may be due to sum of two contributions: one is incoherent scattering from solvent, and the other is the scattering from concentration fluctuations between nondeuterated acetonitrile and acetate buffer in D_2O. At the lower q-region of $q < 0.1$ nm^{-1}, however, upturn of the scattered intensity with decreasing q was observed. After the subtraction of q-independent background scattering, the scattering profile at the low q-region reveals an excess scattering due to enzyme expressed by

$$\frac{d\Sigma}{d\Omega}(q) \propto q^{-4} \tag{3}$$

as indicated by the dotted line in Figure 2. This piece of evidence for the enzyme solution was clarified for the first time by the scattering method to our best knowledge.

III.4.2. SANS from Monomer Solution. The SANS profile for monomer solution, containing CH_3CN by the same amount as the reaction solution, is also shown by filled circles in Figure 2. The scattered intensity was almost identical to the scattering from the enzyme solution at the higher q-range of $q \geq 0.1$ nm^{-1}: There seemed to be no excess scattering beyond a sum of the incoherent scattering intensity and the coherent scattering from the small concentration fluctuations as mentioned above. Thus, the monomer solution was clarified to be homogeneous, despite the fact that the monomer substrate had both a hydrophilic and hydrophobic parts.

III.4.3. Time-Resolved SANS during Enzymatic Polymerization Process. Time change in the SANS profiles (unfilled circles) during enzymatic polymerization process was successfully followed for the first time, the result of which is shown in Figure 3. The profile for the enzyme solution was also shown by filled circles as the reference which indicated the scattering before polymerization. Throughout the polymerization process, the scattered intensity distributions $d\Sigma/d\Omega(q)$'s were well fitted by the following equation

$$\frac{d\Sigma}{d\Omega}(q) = Aq^{-\alpha} + B \tag{4}$$

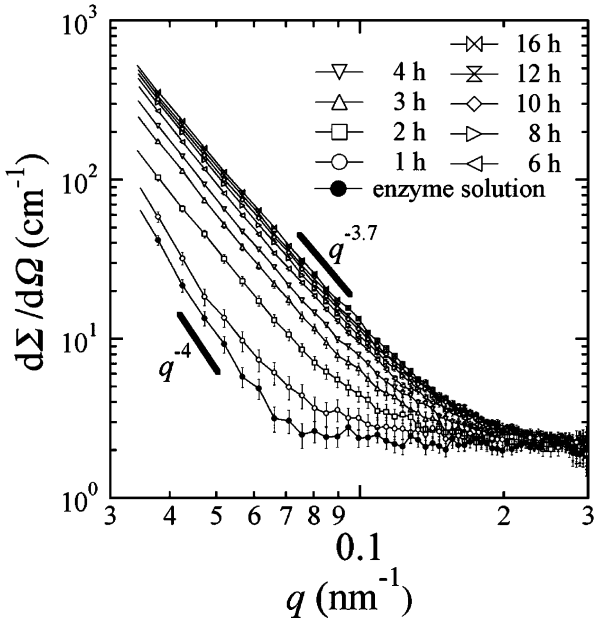

Figure 3. Time evolution of the SANS profiles during enzymatic polymerization process. SANS from enzyme solution was also included as a reference.

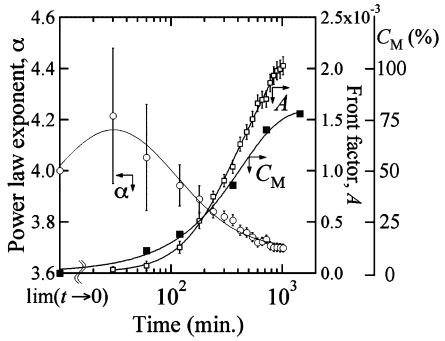

Figure 4. Time change in power law exponent, α, front factor, A, and monomer conversion, C_M.

where A is a front factor, α is the power-law exponent, and B is time-independent constant value, corresponding to the scattered intensity level observed at higher q-range of $q > 0.1$ nm^{-1} in Figure 2, as mentioned in sections III.4.1 and III.4.2. By fitting all the SANS profiles during the polymerization process with eq 4, we can obtain the time change in A (open squares), and α (open circles), as shown in Figure 4. With increasing polymerization time, A increased monotonically, the trend of which was nearly the same as the time change in C_M. On the other hand, α seemed to once increase from 4.0 to 4.2 and then decrease from 4.2 to 3.7 in the course of the polymerization process.

IV. Discussion

IV.1. Structure of Enzyme Solutions. As described in section III.4.1, the upturn of the SANS profile for the enzyme solution given by eq 3 can be rationalized by Porod's law,[22] applicable for systems containing structures having a smooth surface with an infinitesimally thin interfacial boundary. The Porod law could be observed even at the lowest accessible q of $q = 0.03$ nm^{-1}, suggesting that the structures formed in the enzyme solution had characteristic lengths larger than 200 nm, and the surface of the structure was flat over the length scale smaller than 200 nm. In addition, judging from the fact that in Figure 2 the SANS profile for the reaction medium itself showed

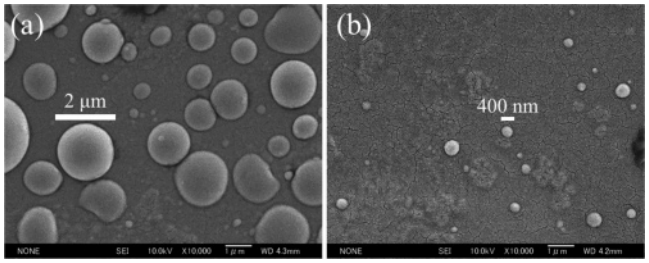

Figure 5. Typical FE-SEM images for the enzyme associations: (a) relatively large associations; (b) relatively small associations.

no excess scattering, the structures in the solution consisted of assemblies of the enzyme molecules. Thus, our SANS results unequivocally elucidated the in-situ existence of the self-assembled enzyme in the reaction medium for the first time. Since the enzyme (cellulase) has both hydrophilic and hydrophobic sequences linked together in its primary molecular architecture, it seems to be natural for the enzyme molecules to form associations in the solution composed of organic and aqueous solvents.

Figure 5a,b shows FE-SEM images for the enzyme associations taken at two representative areas on the silicon substrate (see section II.2.7). The areas where relatively large domains were observed are highlighted in Figure 5a, while in Figure 5b that having relatively small domains. In the images, we can observe spherical domains having diameters ranging from 200 nm to 2 μm. The observed difference in the domain size may be explained as follows. As detailed in section II.2.7, the sample preparation for SEM observations involves the solvent evaporation process, during which the enzyme associations in the solution may coalesce and grow into larger associations. The faster the evaporation process, the less time available for coalescence and growth, giving rise to smaller associations. Therefore, the images in parts a and b of Figure 5 are expected to correspond to the areas subjected to slower and faster evaporation rates, respectively. The image in Figure 5a clearly reveals itself the coalescence-growth process of the enzyme associations.

It should be also noted that the surface of the associations seems smooth, which is perfectly consistent with the SANS result in Figure 2. However, we should notice that the size of the association observed by FE-SEM may not be exactly the same size as that in the solution because of the possibility of growth of the enzyme association during the solvent evaporation process. Thus, we can only conclude the existence of the enzyme association with smooth surface and sharp boundary from the FE-SEM images in a strict sense.

Next we performed the time evolution of the SANS profile from the enzyme solution after the preparation of the solution in order to examine the stability of the enzyme associations themselves in the solution free from monomers. Figure 6 shows the time dependence of the SANS profiles measured at $t = 0-12$ h. All the profiles were found to be almost identical and independent of time, showing the power law behavior of q^{-4}. This indicates that the surface area per unit volume was kept constant for at least for 12 h and hence indicates that average size and the number density of the enzyme associations in the solution should be kept constant, clearly revealing for the first time that the enzyme associations are stable in the reaction medium and do not precipitate.[23]

IV.2. Proposed Specific Reaction Fields To Be Observed by Time-Resolved SANS. Here in this section we shall propose the specific reaction field which creates self-assembling reaction products. Judging from the SANS results for the enzyme

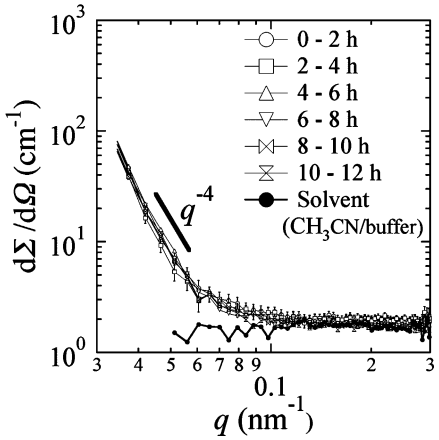

Figure 6. SANS profiles for the enzyme solutions taken as a function of time after preparation of the solution. The scattering from solvent is also shown as a reference.

solution as elucidated in section IV.1, we can visualize the following specific reaction field created by enzyme associations in the reaction medium: Over the length scale (r < 200 nm) covered by the time-resolved SANS, the enzyme association has a flat, smooth surface with a sharp interface boundary against the reaction medium as schematically illustrated in Figure 7a, which is well characterized by the Porod law[22] given by eq 3.

In this work we used an unpurified enzyme which contains only a small fraction of active enzymes for the polymerization (less than 1% of the total enzyme as will be discussed in section V.2). A major fraction of it is inactive for the polymerization. Consequently, the active sites for enzymatic polymerization are statistically far apart in the enzyme association, as schematically shown in part a of Figure 7. Although part a shows only the active ones near the surface of the enzyme association, the active ones would exist also inside the enzyme association. According to information on the contemporary enzyme chemistry,[24,25] upon zooming in the active site in part a, one would see an active enzyme molecule of ~5 nm in diameter[24] (part b). The active enzyme contains a special part of the so-called cleft having ~3 nm length and ~0.5 nm along the cross-sectional directions. Upon a further zoom in part b, the cleft is composed of two subsites, the donor and acceptor sites, bordered at the active center as shown in part c where a substrate monomer is recognized and activated at the donor site for glycosylation reaction (via liberation of HF), and the growing polymer chain, whose chain end is linked to the active center, is located at the acceptor site.[26,27]

In the context of the information given above, we propose it is important to visualize the enzymatic polymerization at the two subsites as follows: (i) Monomer reaction: The monomers (having a characteristic length of ~1 nm) diffuse into the donor site from the reaction medium, driven by a concentration difference of the monomer such that concentration of the monomers is large in the reaction medium outside the enzyme association but is small in the donor site. In addition to this mechanism, the monomers may be also driven into the donor site assisted by some specific supramolecular interactions with the active enzyme. Among the monomers driven to the donor site, only the monomers having a proper orientation may be recognized and activated there and reacted (chemically linked via glycosylation reaction by the catalytic action of the active center) with a growing polymer chain located at the acceptor site. (ii) Polymer reaction: The polymer chain grown by one monomer unit longer due to the glycosylation shifts along the narrow confined space of the acceptor site in the cleft. The

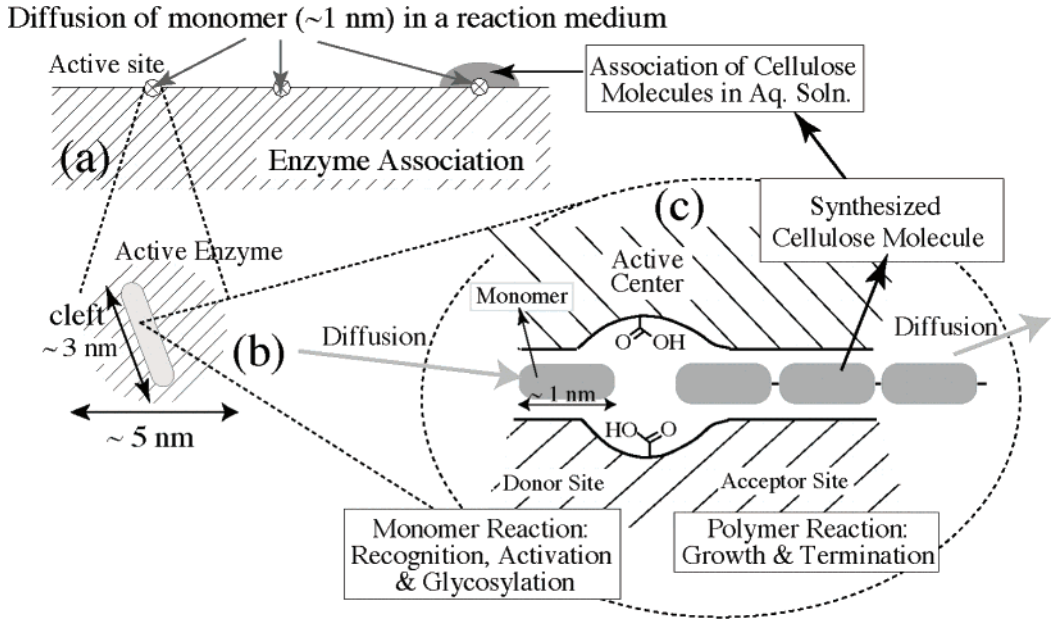

Figure 7. Schematic illustration of a specific reaction field of enzyme associations to be observed by the combined SAS method.

repetition of steps i and ii is a propagation (growing) reaction.

With help of basic polymer physics we may be able to advance our thoughts about the polymer growth and termination processes by a step further and to propose a conjecture as follows. As polymers grow, the local concentration of the polymers in the reaction field of the very narrow confined space (around the acceptor site) must become extremely large. On the other hand, the polymer concentration in the space outside of the reaction field (in the reaction medium shown in Figure 7a) would be kept always very small for the reason as will be discussed in the next paragraph. The large concentration difference of the polymer between these two regions would drive the growing polymer chain away from the active center toward the reaction medium. Thus, the growing polymer chain may be forced to be detached from the active center and to diffuse outside the enzyme associations. The polymer chain brought away from the active center is no longer active for the polymerization and hence *reaction-terminated*, and another cycle starts to produce another polymer at the same active center. This cycle is repeated, and as a consequence one active enzyme forms a numerous number of the cellulose molecules, as will be detailed in section V.2. From the point of view as described above, we believe it is reasonable to consider the termination process is stochastic and controlled by the physical factors, though this point has not been explicitly mentioned earlier in the field of both in-vitro and in-vivo synthesis of cellulose. The stochastic termination process may be evidenced by the relatively low molecular weight of the product.

Each active site creates a large number of cellulose molecules, as will be summarized in section V.2. The synthesized cellulose molecules are not soluble in the reaction medium and hence associate themselves via hydrogen bonding, giving rise to self-assembling structures around the surface of the enzyme associations, as also shown schematically on the right-top corner in Figure 7a. The association of thus as-synthesized cellulose molecules into cellulose fibrils should always keep the local concentration of cellulose molecules dissolved in the reaction medium very low, which promotes the synthesized cellulose molecules to spring out from the acceptor site to the reaction medium via the diffusion driven by the concentration difference of the polymers as described above.

The chemical reaction would occur also at the active site of the enzyme located inside the enzyme association, as long as the active enzyme kept the catalytic activity for the polymerization. In this case, the growing cellulose fibrils formed by the as-synthesized polymers, which are kept being created at the active enzyme, may break the enzyme association and create a new surface for the enzyme association in order for the active enzyme to keep its catalytic activity. Otherwise, the acceptor site would be crammed with the synthesized cellulose molecules, resulting in the loss of the catalytic activity. Thus, the growth of the cellulose aggregates around the surface and the interior of the enzyme association will end up to cover the surface of the enzyme association, as will be shown in Figure 12d.

The time-resolved SANS will explore the time evolution of such self-assembling process of the as-synthesized cellulose molecules as described above. It should be noted that the model for the cellulose association on the top right corner of the enzyme association (Figure 7a) demonstrates only in the very early stage of the polymerization process.

IV.3. Interpretation of Time-Resolved SANS Measurement. IV.3.1. At Early Stage of Polymerization ($0 < t < 60$ min). As shown in Figure 4, in this time period, the exponent α in eq 4 showed values apparently larger than 4.0, indicating a possibility that structures may have a diffuse interfacial boundary, in contrast to the situation for the enzyme solution discussed in section IV.1. When α is apparently larger than 4.0, the scattered intensity may be explained by the following equation[28]

$$\frac{d\Sigma}{d\Omega}(q) \propto q^{-4} \exp(-\sigma^2 q^2) \tag{5}$$

as the term $\exp(-\sigma^2 q^2)$ tends to give the exponent α in eq 4 greater than 4, when $\sigma q > 1$, over the limited range of q covered in our experiment. Here σ is related to the characteristic interfacial thickness,[29,30] t, as follows:

$$t = \sqrt{2\pi}\sigma \tag{6}$$

However, as we can see in Figure 4, the values α at $t = 30$ and 60 min have quite a large error bar. Therefore, we would like to just point out the diffuse boundary as a possibility for $\alpha >$

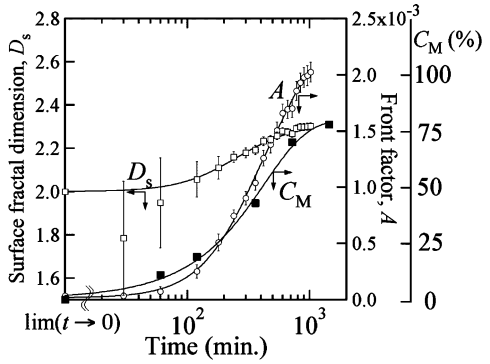

Figure 8. Time change in surface characteristics (fractal dimension, D_s, and A) and monomer conversion, C_M.

4. Nevertheless, if this is the case, this suggests an important physics such that the synthesized cellulose molecules sprung out from the active sites toward the reaction medium can wet and spread on the hydrophobic part of the surface of the enzyme associations ("lateral diffusion"), forming brush layers of cellulose molecules adsorbed on the surface. Note here once again that the enzyme comprises both hydrophilic proteins and hydrophobic proteins, as described in section IV.1.

IV.3.2. At Intermediate and Late Stage of Polymerization ($t \geq 60$ min). At $t \geq 60$ min, the value α was found to be between 3.7 and 4.0. This characteristic power law behavior is explained from the viewpoint of surface fractal.[31,32] The small-angle scattering from surface fractal objects may be written by the following equation proposed by Wong et al.[32]

$$I(q) = \frac{\pi\rho^2 S_2 l_2^{D_s-2}\Gamma(5-D_s)\sin[\pi(3-D_s)/2]}{(3-D_s)q^{6-D_s}} \qquad (7)$$

where ρ and D_s indicate a scattering contrast of the objects against their surrounding medium and their surface fractal dimension, respectively. S_2 and l_2 are defined as follows: S_2 characterized by the smooth surface area measured with a resolution l_2, where l_2 denotes the lower cutoff length of self-similarity. $\Gamma(x)$ indicates a Gamma function of x defined by

$$\Gamma(x) = \int_0^\infty t^{x-1}e^{-x}\,dx \qquad (8)$$

By comparing eq 7 with eq 4, it is found that α and A is rewritten with D_s as

$$D_s = 6 - \alpha \qquad (9)$$

$$A = \frac{\pi\rho^2 S_2 l_2^{D_s-2}\Gamma(5-D_s)\sin[\pi(3-D_s)/2]}{3-D_s} \qquad (10)$$

Thus, by using eq 9, we can estimate a time change in D_s from a time change in α in Figure 4.

Figure 8 shows time change in D_s, A, and C_M. At $t = 0$, D_s was 2.0, reflecting the smooth surface of the enzyme association itself as clarified in section IV.1. Between $0 < t < 60$ min, D_s superficially appears to be less than 2.0 (see the trend shown by unfilled square symbols) as pointed out in section IV.3, probably because the structures with diffuse interfacial boundary may be formed. If this is the case, we cannot define D_s. At $t >$ 60 min, D_s seems to increase from 2.0 to 2.3 with increasing reaction time.[1] This means that as the polymerization proceeds, the surface of the enzyme association becomes rougher with time due to self-assembled structure of as-synthesized cellulose molecules formed around the enzyme association. The appearance of the surface fractal structure may be understood from the viewpoint of diffusion-limited aggregation (DLA) of an enormous number of the synthesized cellulose molecules created via the reactions at the specific sites with a high turnover number, and moreover, this hypothesis is also supported by a Monte Carlo simulation.[33] The time-resolved SANS studies elucidated for the first time this intriguing self-assembling process and structure for the chemically reacting system.

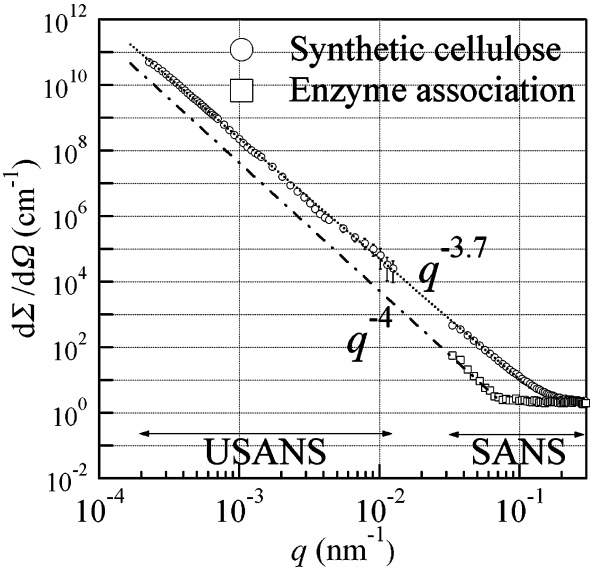

Figure 9. USANS and SANS profiles before (dash-dotted line and squares) and after polymerization (dotted line and open circles).

IV.4. Further Analysis of the Self-Assembly of the Synthetic Cellulose. IV.4.1. USANS and SANS Analyses. In the next step, we like to elucidate the lower and upper cutoff length of the obtained self-similar surface roughness of the aggregates of synthetic cellulose molecules around the enzyme association. For this purpose, we performed static USANS and SANS measurements for the reaction products obtained at 24 h after the onset of the polymerization with the reaction-terminated solution as described in section II.1.

The results are shown in Figure 9, where the SANS profile for enzyme solution was also shown by unfilled squares and the dash-dotted line for comparison. As already explained in section IV.1, it is characterized by $d\Sigma/d\Omega(q) \propto q^{-4}$ (the dash-dotted line in Figure 9) at $0.03 < q < 0.1$ nm^{-1}. Because of low concentration of the enzyme solution and the lack of high brilliance of the incident neutron beam, we could not obtain the USANS profile for the enzyme solution with a sufficient statistical precision so that only the extrapolated asymptotic behavior of q^{-4} was indicated at the low q-region of $q < 0.03$ nm^{-1}.

On the other hand, the scattered intensity for the synthetic cellulose was sufficiently high so that we could obtain a USANS profile with a high precision as shown by unfilled circles in Figure 9. It is noteworthy that the power law behavior of $q^{-3.7}$ was found to be extended in the whole q-regions covered by USANS also, $2 \times 10^{-4} < q < 1 \times 10^{-2}$ nm^{-1}. This indicates that an upper cutoff length, ξ_{upper}, of the self-similarity is larger than 30 μm, corresponding to the lowest accessible q, q_{lower}, of $q_{lower} = (2\pi/\xi_{upper}) = 2 \times 10^{-4}$ nm^{-1}. As for the corresponding SANS profile, we can notice that a deviation from power law of $q^{-3.7}$ is evident at $q > 0.1$ nm^{-1}. However, since this deviation is considered to be mainly due to the contribution of the background scattering dominantly arisen from incoherent scattering of the reaction medium to the net scattering, we cannot

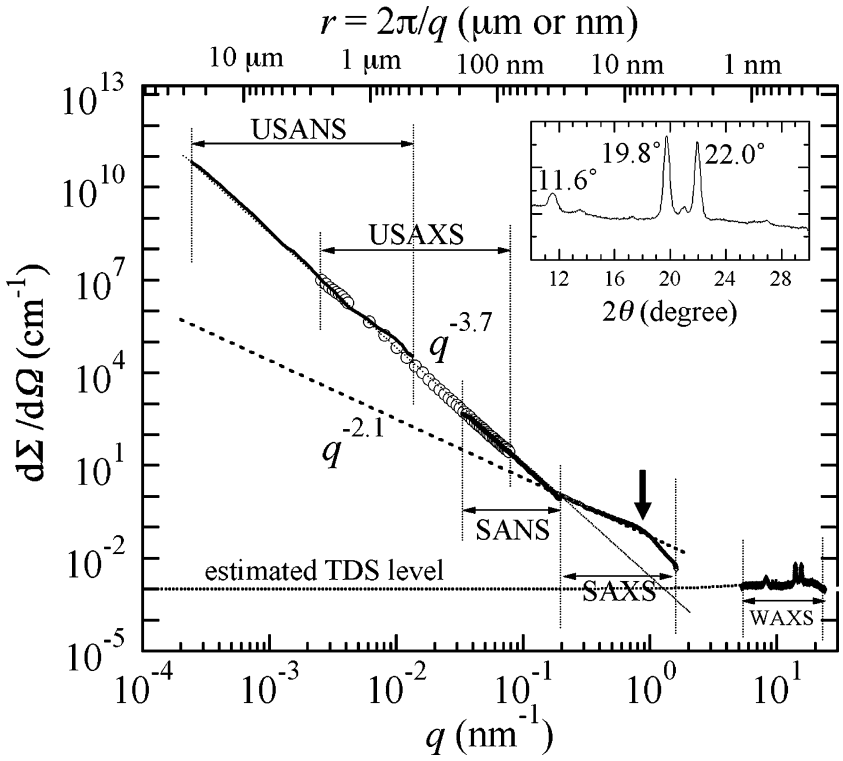

Figure 10. Combined SAS profiles (USANS, USAXS, SANS, and SAXS) and WAXS profile obtained for the in-vitro enzymatic polymerization system, which was reaction-terminated at 24 h after onset of the polymerization. Inset shows enlarged WAXS profile, where 2θ is the Bragg angle.

correctly estimate the lower cutoff length from the SANS profile alone.

IV.4.2. USANS, USAXS, SAXS, SANS, and WAXS Analyses. In order to overcome the difficulty in determining the lower cutoff length from the SANS measurement or to unveil the structure factor hidden by the background scattering level of the SANS at $q > 0.1$ nm^{-1}, we further performed SAXS and WAXS measurements. By combining the two scattering measurements, we succeeded in overcoming the problem attributed to the background scattering encountered in the SANS measurements. Figure 10 shows all the scattering profiles combined together for the same sample specimen as described in the previous section in conjunction with Figure 9. In Figure 10, the two bold lines correspond to the USANS and SANS profiles shown already in Figure 9, and the profiles shown by symbols correspond to the newly added USAXS, SAXS, and WAXS profiles; The USAXS profile fill the gap of the q-region covered by USANS and SANS. In the case of X-ray scattering the thermal diffuse scattering (TDS)[34] dominantly contributes to the background scattering at a high q-region. We can qualitatively estimate the TDS level from the WAXS profile, as shown by the dotted line in Figure 10. Compared with the intensity level of the SAXS profile, the estimated TDS level seems to be lower than the SAXS intensity by about 10−100 times and has almost no contribution to the SAXS profile at $q < 1.4$ nm^{-1}. Thus, we can discuss the lower cutoff length directly from the SAXS profile.

The SAXS profile showed the deviation from the power law of $q^{-3.7}$ at $q = 0.2$ nm^{-1}. At $q > 0.2$ nm^{-1}, the power law may be expressed by $q^{-2.1}$, though the q-range over which the power law is valid is quite narrow, and thereby this power law and its exponent may not be so reliable as the power law of $q^{-3.7}$. This specific power law of $q^{-2.1}$, if it is valid, may be interpreted by a mass fractal structure with mass fractal dimension $D_m = 2.1$, which represents internal structures of the self-assembly[35−37] and reflects a spatial distribution of center of mass of cellulose fibrils. At around $q = 1.0$ nm^{-1}, we can see a broad peak as indicated by a thick arrow. This peak may presumably arise from a long period for stacks of the cellulose crystallites. Thus, from SAXS, an apparent lower cutoff length, $\xi_{lower,a}$, may be estimated to be $\xi_{lower,a} = (2\pi/0.2) = 30$ nm.[38]

By the combined SAS studies covering the wide q-range as wide as 5 orders of magnitude, we discovered that (a) the self-similarity of the surface roughness is extending from 30 nm (though the value being apparent one) to ∼30 μm, over 3 orders of magnitude at least; (b) the long period of the crystallites is ∼6 nm; and (c) the crystal structure of the self-assembled cellulose is a stable one (cellulose II), a possible interpretation of which will be presented in section VI. Result (a) is truly striking because so far there have been almost no reports that successfully observed the self-similar surface roughness extending over such a remarkably wide length scale.

IV.4.3. Real-Space Analysis by FE-SEM. In order to confirm further the surprise on the surface structures as revealed by the scattering studies (the discovery (a)) in the previous section, FE-SEM observations were performed.

Figure 11a−c shows typical FE-SEM images for the synthetic cellulose, taken at three different magnifications. Figure 11a shows an image observed at the lowest magnification (×1000) in this study, where we can see an aggregation of the synthetic cellulose, whose surface seems obviously rougher compared with the image shown in Figure 5. Figure 11b presents an image which focuses and zooms in the central region of the image in part a encompassed by the white rectangle, taken with higher magnification (×10 000) than part a. In part b, we can again confirm the rough surface of the aggregation having almost the same statistical characteristic as in part a. In part b the region encompassed by the white rectangle appears to be smooth. However, a further enlarged view of this part is shown in part c. Surprisingly enough, the self-similar rough surface structure can be clearly observed in the figure. The sizes of the largest and smallest surface structural elements are estimated to be about

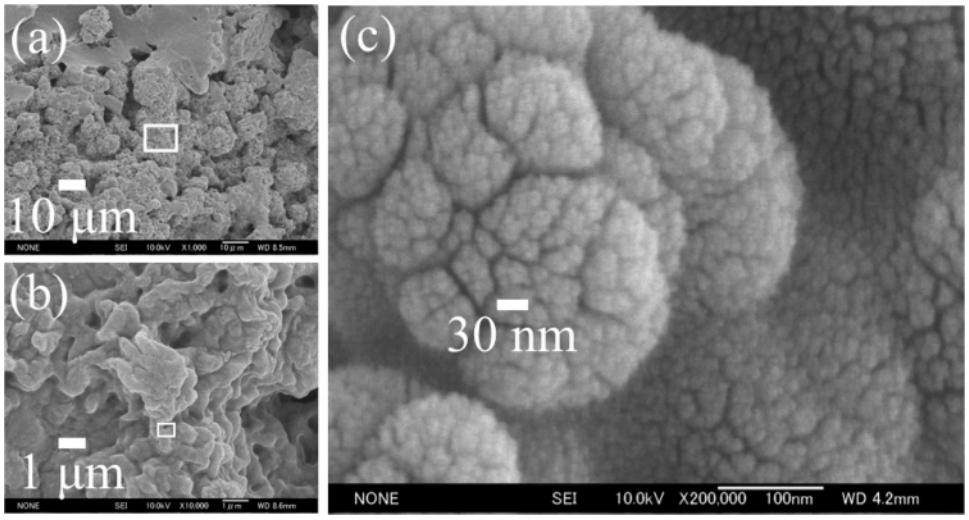

Figure 11. FE-SEM images for the self-assembled synthetic cellulose molecules obtained with three different magnifications.

30 μm and 30 nm from parts a and c, respectively, consistent with the upper and lower cutoff length unveiled by the SAS studies (section IV.4.2), respectively. The self-similar surface structure of the synthetic cellulose is thus successfully captured by the FE-SEM observations also.

V. Summary of Reaction-Induced Self-Assembling Process of Cellulose

V.1. Self-Assembling Process and Structure. Figure 12a−e summarizes schematically the self-assembly of synthesized cellulose molecules. Here it is important to note that the specific reaction fields would play crucial roles to control the polymerization reaction as well as the self-assembly of the reaction products, as discussed in section IV.2.

The SANS and FE-SEM results revealed that the enzyme associations are round and have size of more than 200 nm in diameter and smooth interface with a sharp interfacial boundary (Figure 12a). In the figure we depict the enzyme association at the length scale greater than 200 nm so that a curved surface of the association can be recognized. The active sites are located statistically far apart on the surface as shown in part a because unpurified enzymes were used in this study; they should locate in the interior of the enzyme association also, though not shown in part a.

A great number of polymers having number-average DP of 5.7 with respect to the cellobiose units are created repeatedly from each active site in the enzyme association. The synthesized polymers are expected to spring out from each active sites to the reaction medium outside the surface of the enzyme association, as depicted schematically in part b. Consequently, particular portions of surface of enzyme associations are enriched by the polymers which should diffuse away from the specific portions, along the direction normal to the interface driven by the concentration gradient of the polymers (longitudinal diffusion) and parallel to the interface driven by the wetting (lateral diffusion) as discussed earlier in section IV.3.1. These diffusions in turn create an average concentration gradient of cellulose molecules along the direction normal to the interface of the enzyme association such that the concentration decays with a distance from the interface.

The polymers sprung out on the surface of the enzyme association cannot be dissolved in the reaction medium and hence associate themselves into the aggregates driven by the DLA process around the surface of the enzyme association, as schematically depicted in part c. In the long time limit of the polymerization process, the self-assembled structure of cellulose forms a fractal surface ($D_s = 2.3$) as schematically illustrated in parts c and d. The interior of the object seemingly has mass fractal arrangement of cellulose fibrils ($D_m = 2.1$) as discussed in section IV.4.2 and in ref 33 and depicted to the insets to parts c and d. The cellulose aggregates surrounding the enzyme association are composed of crystalline fibrils organized in the dendritic structures as a consequence of the aggregation driven by the DLA process, as shown in the inset to parts c and d as well as in part e. Part e schematically illustrate a zoom-in picture around the interface between the enzyme association and the cellulose association. Consequently, the cellulose association still have enough free space for the monomers to freely diffuse into the active site from the reaction medium and for the reaction-terminated polymers to diffuse out from the active sites to the reaction medium outside the enzyme association, both driven by the concentration difference of the monomers and the polymers between the two regions, the reaction medium and the active center. Therefore, the polymerization can further proceed under existence of the cellulose aggregates, and as a consequence the cellulose aggregates keep growing as long as the monomers remain to exist. According to our crude estimation, an average volume fraction of polymers dissolved in the reaction medium is much lower than $\sim 1.0 \times 10^{-3}$, as will be detailed in section V.3. In the end of the polymerization reaction the enzyme association is completely covered by the aggregate of the cellulose molecules, as schematically shown in part d.

The scenario described above may explain why the cellulose aggregates to wrap around the enzyme association as shown from parts a−d on the basis of the chemical reaction and the reaction-induced self-assembly of the reaction products at the active enzymes around the surface of the enzyme association. It is also important to consider another scenario, as described earlier in section IV.2, on the basis of the chemical reaction and the reaction-induced self-assembly of the reaction products at the active enzymes inside the enzyme association. The self-assembly of the cellulose molecules into the cellulose fibrils and the growth of the fibrils inside the enzyme association may break the enzyme association and create a new surface of the enzyme association. This process also gives rise to the process from parts b−d shown in Figure 12.

An important question still remained to be addressed is how large is the volume of cellulose aggregates which wraps an active enzyme or an enzyme association. We shall give a crude estimation of it immediately below.

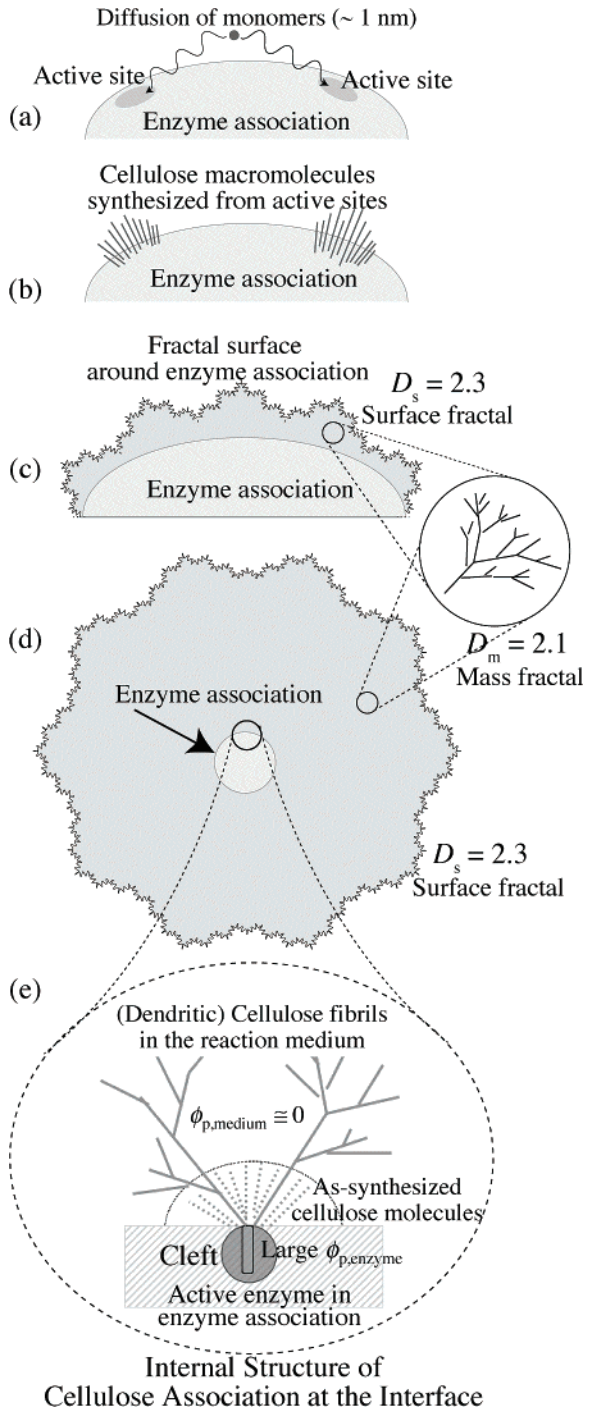

Figure 12. Schematic model of self-assembling process of synthetic cellulose on the surface of enzyme associations. The weight ratios r_w^a and r_w^c of the cellulose created per an active enzyme and per a crude enzyme in the final stage of polymerization are 1.4×10^4 and 14, respectively, as discussed in section V.2. The cellulose aggregate surrounding the enzyme association has enough free space for diffusion of monomers from the reaction medium into the active sites and for diffusion of terminated polymers from the active sites into the reaction medium as discussed in section V.3.

V.2. Estimation of Total Turnover Number, $N^a_{t,cellulose}$. We can roughly make an order estimation of a total number of cellulose molecules $N^a_{t,cellulose}$ created per an active enzyme during the whole reaction process based upon information obtained from the experimental conditions: substrate monomer concentration [M], C_M, DP, concentration of total amount of enzyme $[E]_n$ (g/L), a number fraction of active enzyme f_a, and molecular weight of enzyme M_{enz}. Among these parameters, f_a is the only one which is difficult to be estimated. Nevertheless, we estimated f_a to be 0.1% from a weight loss during the purification procedures of the crude enzyme: To obtain the active enzyme with assaying the polymerization process,[14] the total weight of the starting enzyme was much reduced to less than 1 wt % (approximately around 0.1 wt %) after isolation of the purified active enzyme fraction. The superscript a in X^a refers hereafter to the quantity X per active enzyme. The detailed manipulation yielded $N^a_{t,cellulose} \cong 3 \times 10^5$, as reported in ref 17 in the previous paper.[1] The weight ratio r^a_w of the amount of synthesized cellulose molecules to the amount of the active enzyme was estimated as $r^a_w = 1.4 \times 10^4$, as also reported previously.[1] Similarly the volume ratio r^a_w of the volume of synthesized cellulose molecules to the volume of active enzyme can be estimated as $r^a_v \cong 1.7 \times 10^3$ where the synthesized cellulose molecules are assumed to be rigid and to have a cylindrical shape (because of a uniform rotation of the molecules around its axis) having radius 0.15 nm and length 5.7 nm, while the active enzyme is the sphere of radius 2.5 nm.

$N^c_{t,cellulose}$, r^c_w, and r^c_v per crude enzyme can be respectively estimated by multiplying $N^a_{t,cellulose}$, r^a_w, and r^a_v by f_a. The results of such a manipulation yield $N^c_{t,cellulose} = 2.8 \times 10^2$, $r^c_w = 14$, and $r^c_v = 1.7$. If we assume the crude enzyme forms a core sphere of radius $R_{e,c}$, upon which cellulose molecules aggregate as a shell of thickness $R_{net} - R_{e,c}$ where R_{net} is a net radius of the core−shell sphere, we obtain $R_{net}/R_{e,c} = 2.6$, in the case when volume fraction of cellulose in the shell is 10%. The schematic diagram in Figure 12d was drawn on the basis of the above crude estimation.

V.3. Estimation of Volume Fraction of Cellulose Molecules in Their Self-Assembly. The average volume fraction of the synthesized cellulose molecules in the solution ϕ was also estimated previously (see ref 19 in the previous paper[1]): The result gave $\phi \cong 0.79 \times 10^{-3}$. This value of ϕ was calculated under the assumption that all the cellulose molecules synthesized are uniformly dissolved in the reaction medium as a whole. However, the cellulose molecules actually form aggregates around the surface of the enzyme association. Therefore, the effective concentration of the synthesized cellulose molecules dissolved in the reaction medium is always kept much lower than the ϕ value and thereby kept very low. This enables the synthesized cellulose molecules to continue to spring out from the reaction-field around the acceptor site to the reaction medium even under the situation where bulky aggregates of cellulose are wrapping the enzyme association in the reaction medium.

VI. Perspectives

Here we like to touch a possibility on how to overcome the problem that the present enzymatic polymerization can create cellulose molecules having low DP only (as much as 11 cellobiose units[9]). As pointed out in section IV.2, this polymerization involves the monomer reaction (recognition, activation, and glycosylation) at the donor site and the polymer reaction (growth and termination) at the acceptor site. Key factors to affect DP of the synthesized polymer should exist in these two reaction processes. The previous works already implied some hints on this point by showing that yield of the reaction products depends largely on composition of organic solvent and acetate buffer as well as type of organic solvents used as a reaction medium.[9]

Probably, much more precise control of the thermodynamic parameters of the reaction medium (including the possibility of adding a surfactant) than the one previously tried[9] will be crucial to attain much higher DP values. This is because the

local concentration of polymer, $\phi_{p,enzyme}$, in the narrow confined region of the specific site (around the acceptor site and its surrounding region) becomes extremely high, as shown in Figure 12e. However, the local concentration of the cellulose molecules dissolved in the reaction medium, $\phi_{p,medium}$, should be extremely low in the present system, as also shown in Figure 12e, because as-synthesized cellulose molecules around the surface of the enzyme association will be soon associated in the cellulose fibrils due to the poor solvent quality. The large concentration difference of the cellulose molecules dissolved in these regions, $\Delta\phi_p \equiv \phi_{p,enzyme} - \phi_{p,medium}$, would force the growing cellulose molecule to detach from the active center and to diffuse out from the acceptor site in the active enzyme toward the reaction medium and thus to terminate the propagation reaction. If the solvent quality for the synthesized cellulose molecules is improved, $\Delta\phi_p$ becomes less. The lowered $\Delta\phi_p$ will reduce the force to detach the growing cellulose molecule from the active center and hence slow down the termination rate, which in turn will increase molecular weight of the polymer.

Consequently, miscibility of the synthesized cellulose molecules in the reaction medium comes into a play, and hence the precise control of thermodynamic parameters becomes very important. One of the thermodynamic parameters will be polymerization temperature. However, temperature cannot be changed so widely because at extremely high or low temperature ($T > 40$ °C or $T < 10$ °C) enzyme molecules will lose their activity for polymerization reaction. Another possible parameter which can be changed may be pressure. As an outstanding merit of using pressure as a variable, in contrast to varying composition of mixed solvents, one can more "continuously" and "precisely" control thermodynamic property of the reaction medium. The studies along this line deserve future works. Another way to raise molecular weight of the polymer may be to increase a reaction rate of the monomer for the complex formation with the enzyme. However, it is difficult to figure out effective ways to accomplish this at the moment.

Finally, we like to add our comment on crystal structure developed in the in-vitro enzymatic polymerization. With the unpurified enzymes used in this work we could observe only the thermodynamically stable crystal structure (cellulose II). We interpret that this may be attributed to such an effect that a rotational diffusion of the cellulose molecules could occur during the successive formation of the cellulose molecules from an active enzyme. The effect would allow the antiparallel alignment of the molecular axes stabilized by the intermolecular hydrogen bonding in the association process. If the active sites are closely spaced, the cellulose molecules successively formed from the neighboring active sites may associate themselves with the parallel alignment of the molecular axes before their rotational motions occur to attain the antiparallel association. This postulate, which provides a possibility of a kinetically controlled formation of the thermodynamically unstable crystal structure (cellulose I), should be tested in future. Actually, a previous study elucidated that the cellulose I was formed by using purified enzymes which are thought to contain the more closely spaced active sites in the enzyme associations.[14]

VII. Concluding Remarks

We have elucidated physical factors which affect chemical reaction processes at specific sites and reaction-induced self-assembling processes at specific sites by using the system undergoing in-vitro enzymatic synthesis of cellulose as a model system. We proposed an approach to investigate this kind of problem based on real-time analyses of the combined small-angle scattering method together with real-space analyses. The approach proposed and the results obtained here will be applicable to many "open nonequilibrium" systems in nature and biological systems.

Acknowledgment. The authors gratefully acknowledge financial support provided by 21st Century COE Program for a United Approach to New-Material Science. The authors gratefully acknowledge Prof. Benjamin Chu for his invaluable comments on this work and Profs. M. Ohmae and A. Makino for their useful discussions and kind cooperation with our experiments.

References and Notes

(1) Hashimoto, T.; Tanaka, H.; Koizumi, S.; Kurosaki, K.; Ohmae, M.; Kobayashi, S. *Biomacromolecules* **2006**, *7*, 2479−2482.
(2) Schlubach, H. H.; Lührs. L. *Ann. Chem.* **1941**, *547*, 73−85.
(3) Husemann, E.; Müller, G. J. M. *Makromol. Chem.* **1966**, *91*, 212−230.
(4) Schuerch, C. *Adv. Polym. Sci.* **1972**, *10*, 173−194.
(5) Micheel, F.; Brodde, O-E.; Reinking, K. *Liebigs. Ann. Chem.* **1974**, 124−136.
(6) Uryu, T.; Yamaguchi, C.; Morikawa, K.; Terui, K.; Kanai, T.; Matsuzaki, K. *Macromolecules* **1985**, *18*, 599−605.
(7) Colvin, J. R. *Nature (London)* **1959**, *183*, 1135−1136.
(8) Elbein, A. D.; Barber, G. A.; Hassid, W. Z. *J. Am. Chem. Soc.* **1964**, *86*, 309−310.
(9) Kobayashi, S.; Kashiwa, K.; Kawasaki, T.; Shoda, S. *J. Am. Chem. Soc.* **1991**, *113*, 3079−3084.
(10) In carbohydrate chemistry, a "polysaccharide" refers to a compound having more than 10 monosaccharide units: Kennedy, J. F.; White, C. A. Polysaccharides. In *Comprehensive Organic Chemistry*; Barton, D., Ollis, W. D., Haslam, E., Eds.; Pergamon Press: Oxford 1979; Vol. 5, pp 755−830. According to this definition, the product synthesized in this study belongs to cellulose, a typical polysaccharide family.
(11) Kobayashi, S.; Uyama, H.; Kimura, S. *Chem. Rev.* **2001**, *101*, 3793−3818.
(12) Kobayashi, S.; Ohmae, M. *Adv. Polym. Sci.* **2006**, *194*, 159−210.
(13) Kobayashi, S.; Hobson, L. J.; Sakamoto, J.; Kimura, S.; Sugiyama, J.; Imai, T.; Itoh, T. *Biomacromolecules* **2000**, *1*, 168−173.
(14) Lee, J. E.; Brown, R. M., Jr.; Kuga, S.; Shoda, S.; Kobayashi, S. *Proc. Natl. Acad. Sci. U.S.A.* **1994**, *91*, 7425−7429.
(15) Tanaka, H. Ph.D. Dissertation, Kyoto University, Kyoto, Japan, 2007.
(16) Bonse, U.; Hart, M. *Appl. Phys. Lett.* **1965**, *7*, 238−240.
(17) Yamaguchi, D.; Koizumi, S.; Motokawa, R.; Kumada, T.; Aizawa, K.; Hashimoto, T. *Physica B* **2006**, *385*−*386*, 1190−1193.
(18) Koga, T.; Hart, M.; Hashimoto, T. *J. Appl. Crystallogr.* **1996**, *29*, 318−324.
(19) Suehiro, S.; Saijo, K.; Ohta, Y.; Hashimoto, T.; Kawai, H. *Anal. Chim. Acta* **1986**, *189*, 41−56.
(20) Hashimoto, T.; Okamoto, S.; Saijo, K.; Kimishima, K.; Kume, T. *Acta Polym.* **1995**, *46*, 463−470.
(21) Ranby, B. G. *Acta Chem. Scand.* **1952**, *6*, 101−115.
(22) Porod, G. *Kolloid-Z.* **1951**, *124*, 83−114.
(23) The stability of the enzyme associations may be interpreted as a consequence of the balance between (i) an effective binding force between the enzyme associations and (ii) the random thermal force acting on the enzyme associations. The diffusion and coalescence of the enzyme associations may induce a welding of the coalesced associations into a larger association as well as a recoil from coalescence. The effective binding force will decrease with the size of the association because the contact area fraction between the coalesced association will decrease with the size. Therefore, the recoil may outweigh the welding when the size becomes larger than the critical size, which may explain the stability of the enzyme association in the medium.
(24) Davies, G. J.; Dauter, M.; Brzozowski, M.; Bjørnvad, H. E.; Anderssen, K. V.; Schülein, M. *Biochemistry* **1998**, *37*, 1926−1932.
(25) Toerroenen, A.; Rouvinen, J. *Biochemistry* **1995**, *34*, 847−856.
(26) Sulzenbacher, G.; Driguez, H.; Henrissat, B.; Schuelein, M.; Davies, G. J. *Biochemistry* **1996**, *35*, 15280−15287.
(27) Aronson, N. N.; Halloran, B. A.; Alexyev, M. F.; Amable, L.; Madura, J. D.; Pasupulati, L.; Worth, C.; Roey, V. P. *Biochem. J.* **2003**, *376*, 87−95.
(28) Ruland, W. *J. Appl. Crystallogr.* **1971**, *4*, 70−73.
(29) Hashimoto, T.; Shibayama, M.; Kawai, H. *Macromolecules* **1980**, *13*, 1237−1247.

(30) Hashimoto, T.; Fujimura, M.; Kawai, H. *Macromolecules* **1980**, *13*, 1660−1669.
(31) Schaefer, D. W.; Bunker, B. C.; Wilcoxon, J. P. *Phys. Rev. Lett.* **1987**, *58*, 284−285.
(32) Wong, P. Z.; Bray, A. J. *J. Appl. Crystallogr.* **1988**, *21*, 786−794.
(33) Kawakatsu, T.; Tanaka, H.; Koizumi, S.; Hashimoto, T. *J. Phys.: Condens. Matter* **2006**, *18*, S2499−S2512.
(34) Rathje, J.; Ruland, W. *Colloid Polym. Sci.* **1976**, *254*, 358−370.
(35) Schaefer, D. W.; Martin, J. E.; Wiltzius, P.; Cannell, D. S. *Phys. Rev. Lett.* **1984**, *52*, 2371−2374.
(36) Schaefer, D. W.; Keefer, K. D. *Phys. Rev. Lett.* **1986**, *56*, 2199−2202.
(37) Freltoft, T.; Kjems, K.; Sinha, S. K. *Phys. Rev. B* **1986**, *33*, 269−275.
(38) There may be a possibility the power law of $d\Sigma/d\Omega(q) \sim q^{-3.7}$ may persists up to the q-region larger than $q = 0.2$ nm^{-1}. If this is the case, the true lower cutoff length ξ_{lower} is smaller than $\xi_{lower,a}$. Whether or not $\xi_{lower,a} = \xi_{lower}$ should be checked by changing the contrast factors of SANS and SAXS or by some other independent experiments.

MA070699U